

## Quantitative modeling of secondary electron emission from slow-ion bombardment on semiconductors

Marnik Bercx,<sup>\*</sup> Bart Partoens, and Dirk Lamoen

*EMAT & CMT groups, Department of Physics, University of Antwerp, Groenenborgerlaan 171, 2020 Antwerp, Belgium*

 (Received 25 April 2018; revised manuscript received 24 September 2018; published 11 February 2019)

When slow ions incident on a surface are neutralized, the excess potential energy is passed on to an electron inside the surface, leading to emission of secondary electrons. The microscopic description of this process, as well as the calculation of the secondary electron yield, is a challenging problem due to its complexity as well as its sensitivity to surface properties. One of the first quantitative descriptions was articulated in the 1950s by Hagstrum, who based his calculation on a parametrization of the density of states of the material. In this paper, we present a model for calculating the secondary electron yield, derived from Hagstrum's initial approach. We use first-principles density functional theory calculations to acquire the necessary input and introduce the concept of electron cascades to Hagstrum's model in order to improve the calculated spectra, as well as remove its reliance on fitting parameters. We apply our model to  $\text{He}^+$  and  $\text{Ne}^+$  ions incident on Ge(111) and Si(111) and obtain yield spectra that match closely to the experimental results of Hagstrum.

DOI: [10.1103/PhysRevB.99.085413](https://doi.org/10.1103/PhysRevB.99.085413)

### I. INTRODUCTION

Secondary electron emission (SEE) is an important phenomenon where electrons of a target material are emitted through the impact of energetic primary particles. Such processes lie at the foundation of several techniques for characterizing surfaces and play an important role in applications such as plasma sputtering deposition [1,2] and plasma display panels [3,4]. For the case of incident ions, measurements of the electron yield  $\gamma$  were first performed by Hagstrum [5,6]. Although there is a considerable need for data on the electron emission from incident ions, e.g., as input for models of microplasmas [7,8], further measurements of  $\gamma$  for semiconductors are limited. This lack of experimental data has led to an increased interest in theoretical modeling of ion-induced secondary electron emission.

One of the first quantitative descriptions of the interaction of incident ions with a surface was also developed by Hagstrum [9,10], who used a model for the density of states in order to derive the yield of secondary electrons emitted from the surface per incoming ion. His approach was relatively successful but required the use of a substantial amount of fitting parameters in order to make his simulations match experiment. Since then, there have been numerous attempts at improving the quantitative modeling of the SEE process. Propst [11] calculated the Auger matrix elements using a WKB approximation for the tunneling process and was one of the first to consider electron-electron interactions for the secondary electrons. Several authors [12–14] have used a jellium model to calculate the Auger neutralization rate for aluminum and sodium, for which the electrons are well described by a free electron gas. More recently, Cho *et al.* [4] have used first-principles density functional theory (DFT) calculations

in combination with Hagstrum's model to determine the SEE coefficients for MgO. However, they used parameters which were fitted for a specific ion-surface combination ( $\text{He}^+ \rightarrow \text{Ge}$ ) and applied them as if they were fixed parameters of the model. A nice overview of the various theoretical models used to describe the neutralization of incoming ions on a surface can be found in a recent review paper by Monreal [15].

In this work, we make several adjustments to Hagstrum's model in order to remove its dependency on fitting parameters and improve the calculated yield spectra. In this way, we aim to provide a quantitative approach to calculating the secondary electron emission from surfaces bombarded by slow ions. Similar to Cho *et al.*, we start by calculating the required model input from first-principles DFT calculations (Sec. III). Next, we take a closer look at the function that determines the probability that an excited electron will escape (Sec. III A) and introduce the concept of electron cascades (Sec. III B) in order to conceptually improve the model. Finally, we calculate the SEE spectra for  $\text{He}^+$  and  $\text{Ne}^+$  ions incident on Ge(111) and Si(111) and find that they correspond well to the experimental results of Hagstrum (Sec. IV).

### II. SECONDARY ELECTRON EMISSION

Secondary electron emission from incident ions can be the result of either kinetic or potential emission mechanisms [16]. For the former, the emission process is driven by the kinetic energy of the incoming ion. Potential electron emission, on the other hand, transfers the potential energy of the incoming ion to an electron that can then be emitted. For slow moving ions, the potential emission mechanism is dominant [17]. Following Hagstrum's description, it is performed using a two-electron Auger process. Here, a distinction must be made between Auger neutralization (AN) and resonance neutralization (RN) followed by Auger de-excitation (AD), see Fig. 1. For AN, an electron from the surface material tunnels directly into

<sup>\*</sup>marnik.bercx@uantwerpen.be

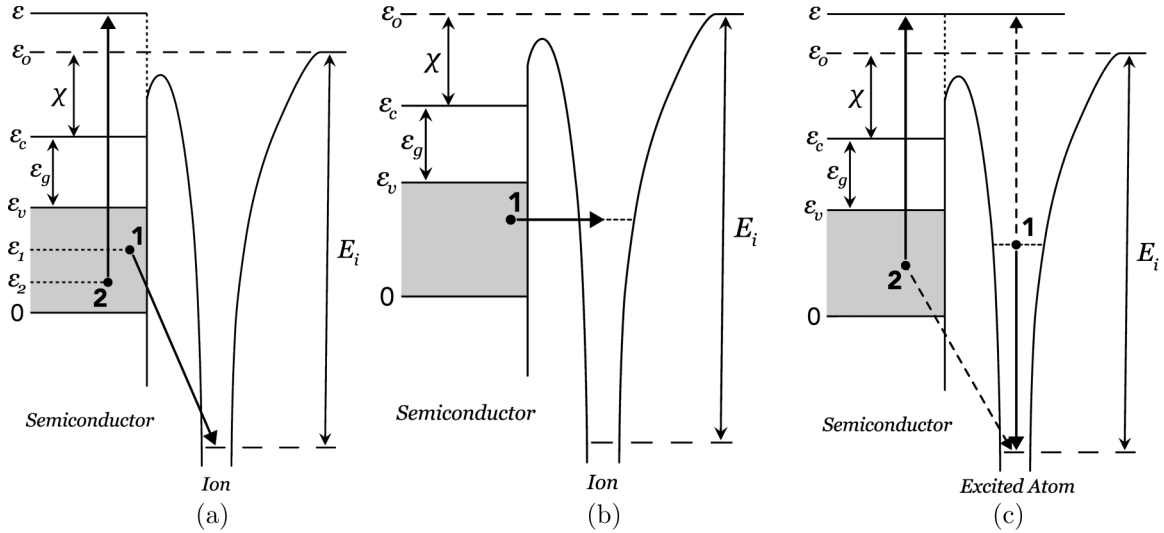


FIG. 1. Schematic representations of the Auger neutralization (a), resonance neutralization (b), and Auger de-excitation (c) processes. For the de-excitation, the set of full and dashed arrows each represent one possible way via which the de-excitation can occur.

the lowest unoccupied state of the incoming ion. The energy released in this transition is passed to another electron in the material. This electron, in turn, has a probability of escape if it is excited to a state with an energy above the vacuum level. In the case of RN, an electron from the surface tunnels into an excited state of the incoming ion, after which the atom returns to the ground state by AD. For slow incident  $\text{He}^+$  and  $\text{Ne}^+$  ions on  $\text{Ge}(111)$  and  $\text{Si}(111)$ , the resonant neutralization channel is unavailable [10,13], so we can safely disregard the RN and AD processes in our discussion.

### A. Hagstrum's model

We begin by presenting Hagstrum's quantitative description of ion-based SEE for semiconductor surfaces, before discussing our adjustments in the sections that follow. During the Auger neutralization, an electron tunnels through the surface barrier to the lowest unoccupied ionic state, transferring the excess energy to a secondary electron of the surface material [Fig. 1(a)]:

$$\varepsilon_1 + \varepsilon_2 \rightarrow \varepsilon + \varepsilon_0 - E_i. \quad (1)$$

Here,  $\varepsilon_1$  and  $\varepsilon_2$  are the initial energies of the electrons of the surface,  $\varepsilon$  is the energy of the excited Auger electron,  $\varepsilon_0$  is the vacuum level, and  $E_i$  the ionization energy of the incoming ion. Determining the transition rates of the various possible transition of the Auger neutralization process involves the calculation of the matrix elements in Fermi's golden rule:

$$\Gamma_{i \rightarrow f} = \frac{2\pi}{\hbar} |H_{i \rightarrow f}|^2 N(\varepsilon), \quad (2)$$

where  $N(\varepsilon)$  is the density of states at the final electron energy,  $\hbar$  is the reduced Planck constant, and  $H_{i \rightarrow f}$  is the transition matrix element:

$$H_{i \rightarrow f} = \int \int u_g^*(\mathbf{r}_1) u_e^*(\mathbf{r}_2) V(\mathbf{r}_1, \mathbf{r}_2) u'_v(\mathbf{r}_2) u''_v(\mathbf{r}_1) d\mathbf{r}_1 d\mathbf{r}_2, \quad (3)$$

with  $u'_v(\mathbf{r}_2)$  and  $u''_v(\mathbf{r}_1)$  the initial states of the electrons in the valence band,  $u_g(\mathbf{r}_1)$  the ground state of the neutralized

ion, and  $u_e(\mathbf{r}_2)$  the excited state of the Auger electron, where  $*$  denotes the complex conjugate. The interaction potential  $V(\mathbf{r}_1, \mathbf{r}_2)$  is the Coulomb potential.

Instead of explicitly calculating the secondary emission yield from the transition matrix elements, as in the earlier work of, e.g., Cobas and Lamb [18], Hagstrum introduced a model based on the density of states (DOS) of the surface. In his approach, the matrix element for each transition is considered to be constant, which means that the probability that an electron of energy  $\varepsilon$  will participate in the Auger neutralization is proportional to the density of states  $N(\varepsilon)$ . In this way, we can simply use the density of states of the surface to calculate the probability that a secondary electron with kinetic energy  $\varepsilon_k = \varepsilon - \varepsilon_0$  is emitted from the impact of an incoming ion. First, the internal distribution of excited electrons  $N_i(\varepsilon)$  is calculated by

$$N_i(\varepsilon) = \frac{D_c(\varepsilon) T \left[ \frac{\varepsilon + \varepsilon_0 - E_i}{2} \right]}{\int_{\varepsilon_c}^{\infty} D_c(\varepsilon) T \left[ \frac{\varepsilon + \varepsilon_0 - E_i}{2} \right] d\varepsilon}, \quad (4)$$

where  $D_c(\varepsilon)$  is the density of the unoccupied states of the surface,  $\varepsilon_c$  the bottom of the conduction band, and  $T$  is the Auger transform:

$$T \left[ \frac{\varepsilon + \varepsilon_0 - E_i}{2} \right] = \int_{\Delta\varepsilon_v} \int_{\Delta\varepsilon_v} D_v(\varepsilon_1) D_v(\varepsilon_2) \times \delta(\varepsilon - \varepsilon_1 - \varepsilon_2 + \varepsilon_0 - E_i) d\varepsilon_1 d\varepsilon_2. \quad (5)$$

Here,  $D_v(\varepsilon)$  is the density of the valence states,  $\Delta\varepsilon_v$  is the valence band width, and  $\delta$  is the Dirac delta function. Note that  $N_i(\varepsilon)$  is normalized to unity because of the assumption that every incoming ion is neutralized, producing one excited electron inside the surface. The delta function is used to assert energy conservation of the Auger neutralization process [Eq. (1)].

Next, the distribution of the electrons that can escape from the surface  $N_0(\varepsilon)$  is calculated by multiplying  $N_i(\varepsilon)$  with the escape probability  $P_e(\varepsilon)$ :

$$N_0(\varepsilon) = P_e(\varepsilon) N_i(\varepsilon). \quad (6)$$

Hagstrum modeled the escape probability  $P_e(\varepsilon)$  using a semi-classical approach, where an electron is considered to be able to escape when the projection of its wave vector on the axis perpendicular to the surface is large enough, i.e., when its corresponding energy is larger than the vacuum level. The resulting escape probability is:

$$P_e(\varepsilon) = \frac{1}{2} \left[ 1 - \left( \frac{\varepsilon_0}{\varepsilon} \right)^\beta \right]^\alpha \quad \text{for } \varepsilon \geq \varepsilon_0, \quad (7)$$

$$= 0 \quad \text{for } \varepsilon < \varepsilon_0,$$

where  $\alpha$  and  $\beta$  represent an anisotropy of the distribution of the initial direction of the wave vector of the electron after excitation. In Hagstrum's approach, these are parameters which are fitted for each ion-surface combination. Finally, the secondary electron yield  $\gamma$ , i.e., the amount of electrons emitted per incoming ion, is calculated by integrating the distribution of escaped electrons:

$$\gamma = \int_{\varepsilon_0}^{\infty} N_0(\varepsilon) d\varepsilon. \quad (8)$$

Using his model, Hagstrum was able to fairly accurately reproduce the yield spectra for  $\text{He}^+$  and  $\text{Ne}^+$  incident on Ge(111) and Si(111). Note that all energies in Eq. (7) are defined with respect to the valence band minimum, which was taken as the zero-energy level by Hagstrum. This corresponds to implicitly deciding on a reference level that determines the effective barrier  $\varepsilon_0$  that the electrons have to pass in order to escape from the surface. Because this reference level affects the probability that an excited electron is emitted, it has a significant influence on the calculated yield.

Although Hagstrum's description of the SEE process was a major step forward, providing an insightful interpretation of his experimental results, he was forced to rely on several fitting parameters in order to be able to reproduce the experimental spectra. Hagstrum had to parametrize the density of states, ionization energy, as well as fit  $\alpha$  and  $\beta$  in the escape function [Eq. (7)]. In our approach, we calculate the density of states from first principles within the DFT framework and remove the parameter dependency of the escape function as described in Sec. III A. For the ionization energy  $E_I$ , we shift the ionization energy of the free atom with the image interaction (2 eV) [19,20]. Finally, we introduce electron-electron scattering as a cascade process in order to improve the calculated yield spectra (Sec. III B).

By virtue of using Hagstrum's model, we are able to include the first-principles calculated electronic structure of the surface, as directly calculating the full matrix elements in Eq. (2) from the DFT wave functions would not be computationally feasible. Several such calculations have been performed for jellium-model wave functions, but this approach would in turn not provide a good description for a semiconductor, nor does it allow us to include the electronic structure of the chosen surface. Gloebl *et al.* [21,22] and Valdès *et al.* [23] did calculate the Auger neutralization rate by considering the matrix elements for the neutralization using a linear combination of atomic orbitals (LCAO) and various distances and positions of an incoming  $\text{He}^+$  ion on several metals and Ge. The electronic response of the surface was modeled using the response function, once again calculated from the jellium

model. They found that the Auger rate was not sensitive to the position of the incoming ion at short distances for Ge, which indicates that considering constant matrix elements is a reasonable approximation for Ge. However, they also found that for noble metals, the presence of d electrons in the valence band that can neutralize the incoming ion has a large effect on the AN rate. The efficient contribution of d electrons compared to s or p states will have to be considered in case the model is extended to be applied to noble metals.

### III. COMPUTATIONAL DETAILS

Hagstrum's model requires the density of states of the valence  $D_v(\varepsilon)$  and conduction  $D_c(\varepsilon)$  band as input, as well as the vacuum level  $\varepsilon_0$ . We calculate the density of states and vacuum level of Ge(111) and Si(111) using a DFT approach, as implemented in the Vienna *ab initio* simulation package [24–27] (VASP). Within the projector augmented wave [28,29] (PAW) formalism, the recommended number of valence electrons is included for both Ge and Si. The energy cutoff is set at 500 eV in order to obtain a well converged plane wave basis set, and the exchange correlation energy is calculated using the Perdew-Burke-Ernzerhof [30] (PBE) functional. A well converged Monkhorst-Pack [31]  $k$ -point mesh is used for sampling the Brillouin zone. We refer the reader to the Supplemental Material [32] for more computational details.

To simulate a surface within the periodic boundary framework of VASP, it is conventional to take a slab approach, where a certain number of atomic layers are separated by a suitably large vacuum layer. For Si and Ge, it is well known that the (111) surfaces reconstruct, forming dimers at the surface with a  $2 \times 1$  periodicity. We take the reconstructed structures from the Supplemental Material of De Waele *et al.* [33] and subsequently optimize the geometry using the computational parameters described in the previous paragraph. The slab consists of 14 atomic layers and at least 20 Å of vacuum spacing is present. The vacuum level is obtained by averaging the one-electron electrostatic potential over planes parallel to the surface and determining the potential in the vacuum, which should be constant in case the vacuum layer is sufficiently thick. The work function  $\phi$  of the surface is then calculated by comparing the vacuum level with the top of the valence band  $\phi = \varepsilon_0 - \varepsilon_v$ .

#### A. The escape function

An integral part of Hagstrum's model is the escape probability function  $P_e(\varepsilon)$ , which represents the probability that an electron at energy  $\varepsilon$  can escape from the surface after excitation. Initially Hagstrum had derived a parameterless expression for  $P_e(\varepsilon)$ , based on an isotropic angular distribution of the wave vector of the excited electrons. However, the resulting distributions of escaped electrons, or yield spectra, did not have sufficient electrons, especially at lower energies. To remedy this, Hagstrum introduced the parameters  $\alpha$  and  $\beta$  [see Eq. (7)], representing an anisotropy of the initial direction of the wave vector of the electron. By fitting these parameters, Hagstrum was able to adjust the escape function and increase the secondary electron yield. Because  $\alpha$  and  $\beta$  are fitted for each ion/surface combination, however, the use of the escape

probability of Hagstrum's model is ill suited for any model that aims to determine the secondary electron emission without relying on experimental input. The approach of Motoyama *et al.* [3] and Cho *et al.* [4], who simply used the fitted parameters for He<sup>+</sup> ions incident on Ge and applied them to other systems, is questionable at best. Finally, Hagstrum's expression for the escape function depends on where we set the zero-energy level. Here, Hagstrum defined all energies with respect to the bottom of the valence band, which results in a low probability of escape due to the relatively large surface barrier.

Instead of Hagstrum's expression for the escape function, we choose to take a quantum mechanical step-barrier approach similar to that of Lorente *et al.* [13]. In this framework, the surface is described as a step function barrier, and the angle-dependent escape probability is derived from the transmission coefficient:

$$P_e(\varepsilon, \theta) = T(k_\perp, p_\perp), \quad (9)$$

where  $\theta$  is the angle between the initial wave vector and the surface normal, and  $k_\perp$  and  $p_\perp$  are the projections of the wave vector on the surface normal inside and outside of the material, i.e.,  $k_\perp = k \cos(\theta)$ . For semiconductors, the barrier is set equal to the electron affinity  $\chi$  [34–36], which corresponds to setting the reference energy level at the bottom of the conduction band  $\varepsilon_c$ . Using this convention, the wave vector is calculated from

$$k = \sqrt{2m_e(\varepsilon - \varepsilon_c)/\hbar^2}, \quad (10)$$

where  $\varepsilon_c$  is the bottom of the conduction band,  $\hbar$  is the reduced Planck constant, and  $m_e$  is the electron mass.  $p_\perp$  is determined using the refraction condition at the surface:

$$\frac{\hbar^2 k_\perp^2}{2m_e} - \chi = \frac{\hbar^2 p_\perp^2}{2m_e}. \quad (11)$$

For a step barrier, the transmission coefficient is given by [13]:

$$T(k_\perp, p_\perp) = \frac{4k_\perp p_\perp}{(k_\perp + p_\perp)^2}. \quad (12)$$

Next, in order to determine the escape probability for an excited electron with energy  $\varepsilon$ , we use the following expression [9]:

$$P_e(\varepsilon) = \int P_e(\varepsilon, \theta) P_\Omega(\varepsilon) d\Omega, \quad (13)$$

where  $P_\Omega(\varepsilon) d\Omega$  is the probability that an electron with energy  $\varepsilon$  has a wave vector  $\mathbf{k}$  with a direction that is part of the solid angle  $d\Omega = \sin\theta d\theta d\varphi$ . If, similar to Hagstrum's initial approach, we assume this distribution to be isotropic, i.e.,  $P_\Omega(\varepsilon) = 1/4\pi$ , and only consider the half sphere in the direction of the vacuum, we obtain:

$$P_e(\varepsilon) = \frac{1}{4\pi} \int_0^{2\pi} d\varphi \int_0^{\frac{\pi}{2}} \sin\theta d\theta \frac{4k_\perp(\theta)p_\perp(\theta)}{(k_\perp(\theta) + p_\perp(\theta))^2}. \quad (14)$$

This expression for the escape function has the advantage that it does not depend on the position of the zero point on the energy axis, since it is calculated using a difference of energy values, i.e.,  $\varepsilon - \varepsilon_c$  in Eq. (10). Moreover, by adopting an isotropic angular distribution for the wave vector of the excited electrons, we avoid the use of the parameters  $\alpha$  and  $\beta$ .

## B. Electron cascades

Using the escape function described in the previous section, we face a similar problem as Hagstrum did when he first considered an isotropic distribution for the wave vectors of the excited electrons: The obtained yield spectra are too low, largely due to an insufficient amount of electrons at lower kinetic energies. This can be seen in Fig. 3, where we have plotted the kinetic energy distribution of the electrons emitted by the initial Auger neutralization. However, the low-energy electrons in the experimental yield spectra are often ascribed in the literature to a mechanism that Hagstrum did not consider in his model, i.e., electron cascades via electron-electron interactions. One of the first to implement this idea was Propst [11], who started from the distribution of electrons that did not escape after the Auger excitation and allowed these electrons to interact with other electrons in the system through scattering events, once again producing electrons that can escape from the surface. He found that 50% of the final yield was produced by the electron cascade process, making it an important contribution to the total yield. The concept has also been considered more recently by other authors, who first described it as an electron cascade process due to its iterative nature. According to Lorente *et al.* [37], the cascading electrons can account for 60% of the total secondary electron emission. Moreover, the electron cascades are found to be the source of the low energy electrons often missing in the calculated yield spectra of computational models.

We introduce our own model for the electron cascade process. Similar to the approach Hagstrum used to calculate the distribution of excited electrons from the neutralization of the incoming ion, we base our implementation of the electron cascades on the energy distributions of the interacting electrons. We begin by considering the energy distribution of the electrons that cannot escape:

$$N_c^{(2)}(\varepsilon) = (1 - P_e(\varepsilon))N_i(\varepsilon). \quad (15)$$

In Hagstrum's model, these electrons simply do not contribute, and their energy has no influence on the SEE yield. Here, we approximate the scattering process using similar assumptions as Hagstrum made for the Auger neutralization, i.e., by considering the matrix elements of the transition to be constant, which makes the probability of a specific scattering event proportional to the density of states at the energy levels involved. The scattering process can be written as:

$$\varepsilon_1 + \varepsilon_2 \rightarrow \varepsilon + \varepsilon', \quad (16)$$

where  $\varepsilon_1$  is the energy of the excited electron before scattering,  $\varepsilon_2$  is the energy of an electron in the valence band, and  $\varepsilon, \varepsilon'$  are the energies of the two electrons after the scattering process (see Fig. 2). The distribution of excited electrons after scattering can then be calculated using:

$$\begin{aligned} N_i^{(2)}(\varepsilon) &\sim \int_{\varepsilon_c}^{\infty} d\varepsilon' \int_{\varepsilon_0}^{\infty} d\varepsilon_1 \int_{\Delta_{\varepsilon_0}} d\varepsilon_2 D_c(\varepsilon) D_c(\varepsilon') \\ &\quad \times N_c^{(2)}(\varepsilon_1) D_v(\varepsilon_2) \delta(\varepsilon + \varepsilon' - \varepsilon_1 - \varepsilon_2) \\ &= D_c(\varepsilon) \int_{\varepsilon_c}^{\infty} d\varepsilon' D_c(\varepsilon') \int_{\varepsilon_0}^{\infty} d\varepsilon_1 \int_{-\infty}^{\infty} d\varepsilon_2 N_c^{(2)}(\varepsilon_1) \\ &\quad \times D_v(\varepsilon_2) \delta(\varepsilon + \varepsilon' - \varepsilon_1 - \varepsilon_2) \end{aligned}$$

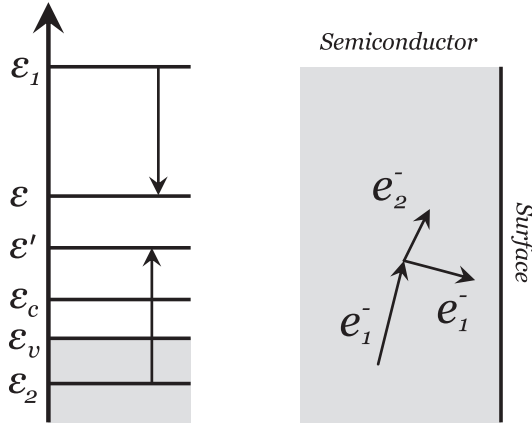


FIG. 2. Energy diagram of a single step in the electron cascade process. The electron at energy  $\varepsilon_1$  scatters on an electron in the valence band at energy  $\varepsilon_2$ , transferring sufficient energy for the second electron to excite into an unoccupied state of the conduction band at energy  $\varepsilon'$ .

$$\begin{aligned}
 &= D_c(\varepsilon) \int_{\varepsilon_c}^{\infty} d\varepsilon' D_c(\varepsilon') \\
 &\quad \times \int_{\varepsilon_0}^{\infty} d\varepsilon_1 N_c^{(2)}(\varepsilon_1) D_v(\varepsilon + \varepsilon' - \varepsilon_1) \\
 &= D_c(\varepsilon) \int_{\varepsilon_c}^{\infty} d\varepsilon' D_c(\varepsilon') T_{ee}(\varepsilon, \varepsilon'), \quad (17)
 \end{aligned}$$

where we have defined the scattering transform  $T_{ee}(\varepsilon, \varepsilon')$  as

$$T_{ee}(\varepsilon, \varepsilon') = \int_{\varepsilon_0}^{\infty} d\varepsilon_1 N_c^{(2)}(\varepsilon_1) D_v(\varepsilon + \varepsilon' - \varepsilon_1). \quad (18)$$

Note that we only consider the excited electrons of  $N_c^{(2)}(\varepsilon)$  above the vacuum energy, as electrons with less energy can no longer produce electrons that can contribute to the secondary electron yield. Finally, because every scattering event results in two excited electrons, we normalize the new distribution of excited electrons to two times the number of electrons above the vacuum energy, prior to the scattering event:

$$N_i^{(2)}(\varepsilon) = 2n_i \frac{D_c(\varepsilon) \int_{\varepsilon_c}^{\infty} d\varepsilon' D_c(\varepsilon') T_{ee}(\varepsilon, \varepsilon')}{\int_{\varepsilon_c}^{\infty} d\varepsilon D_c(\varepsilon) \int_{\varepsilon_c}^{\infty} d\varepsilon' D_c(\varepsilon') T_{ee}(\varepsilon, \varepsilon')}, \quad (19)$$

where

$$n_i = \int_{\varepsilon_0}^{\infty} N_c^{(2)}(\varepsilon') d\varepsilon'. \quad (20)$$

In order to simulate the cascade process, these steps are iterated by adding the escaped electrons  $P_e(\varepsilon)N_i^{(2)}(\varepsilon)$  to the previous yield distribution and once again considering the spectrum of the electrons which cannot escape, from which we calculate the next energy distribution of excited electrons using again the same procedure. These iterations continue until the yield difference between two iterations is smaller than 0.001 electrons per ion. If we apply this approach to the yield calculation of  $\text{He}^+$  ions on Ge(111), we obtain the results in Fig. 3, where we have plotted the number of

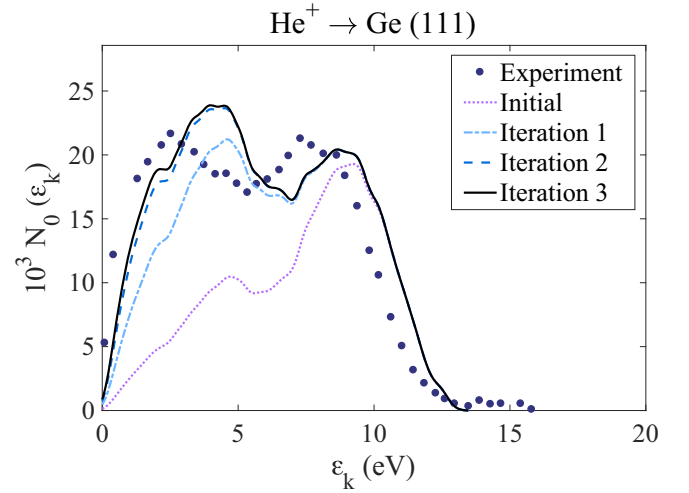


FIG. 3. Calculated distribution of the kinetic energy  $\varepsilon_k$  of secondary electrons emitted for incident  $\text{He}^+$  ions on Ge(111) at various iterations of the electron cascade process.

emitted electrons  $N_0(\varepsilon)$  versus their kinetic energy  $\varepsilon_k$  for several iterations. We can see that as we iterate the electron cascade process, the SEE spectrum quickly converges. The final distribution (iteration 3) has significantly more electrons at lower energies and is a substantial improvement upon the initial yield distribution after Auger neutralization, when compared with the experimental results from Hagstrum [6].

#### IV. RESULTS

The resulting yield spectra for incoming  $\text{He}^+$  and  $\text{Ne}^+$  ions on the reconstructed Ge(111) and Si(111) surfaces are plotted alongside the experimental results of Hagstrum [6] in Fig. 4. In his work, Hagstrum measured the total yield and kinetic energy distribution of the emitted electrons for several energies of the incoming ion on atomically clean, annealed (111) surfaces of Ge and Si. For the experimental results, we have compared our calculated spectra with the results for low energy (10 eV) ions, for which the contribution of kinetic electron emission is negligible, as it is not considered in our model. We can see that overall, the shape of the calculated yield spectra matches reasonably well with the experimental one. The total SEE yield coefficients  $\gamma$ , obtained by integrating the yield spectra [Eq. (8)], are given in Table II. For both Si and Ge, the yield coefficients are larger for  $\text{He}^+$  than for  $\text{Ne}^+$ , due to the larger ionization energy of helium. We also observe that the yield is found to be lower for Si(111) than Ge(111). The calculated yield coefficients are in fair agreement with the experimental values, with a slight overestimation for  $\text{He}^+$  on Ge(111) and underestimation for Si(111).

For Ge(111), the high energy tail of the calculated spectrum is shifted slightly to higher energies, whereas for Si(111), the tail is shifted in the opposite direction. These discrepancies can be attributed to the error on the calculated work function, which are compared with experiment for the Si(111) and Ge(111) surfaces in Table I. We can see that the calculated work function is lower than the experimental result for Ge(111) and slightly higher for Si(111). Because

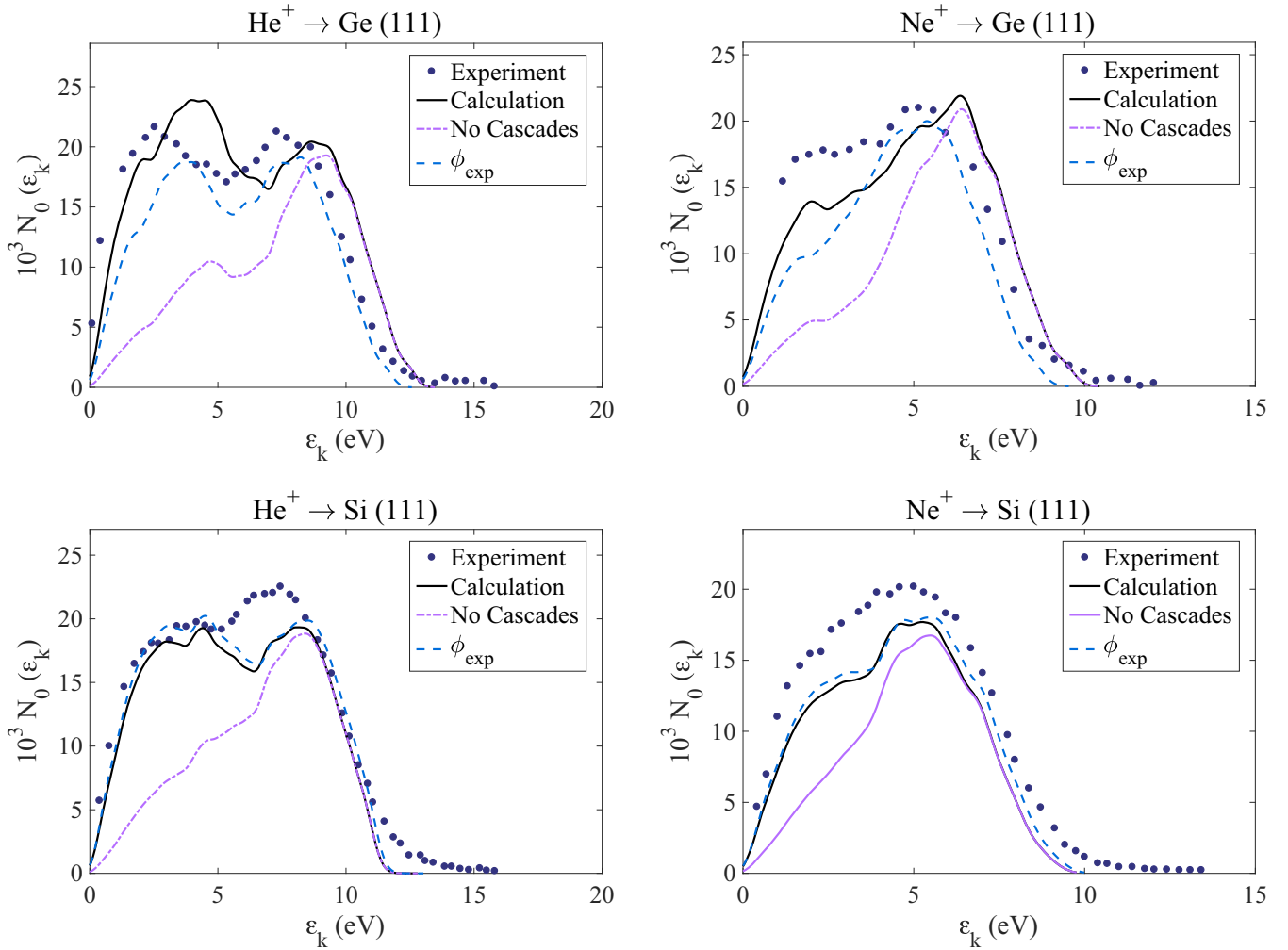


FIG. 4. Experimental and calculated yield spectra for incoming  $\text{He}^+$  and  $\text{Ne}^+$  ions on Ge(111) and Si(111) surfaces. Also shown are the initial yield spectra, i.e., without the addition of the electron cascades process described in Sec. III B, as well as the calculated yield spectra when the vacuum level is adjusted using the experimental values for the work function in Table I.

the vacuum level determines the probability that an excited electron can escape, the work function has a significant influence on the calculated yield. This influence becomes clear when we look at the yield spectra calculated when adjusting the vacuum level to the experimental work function, also plotted in Fig. 4. It is clear that by increasing the work function of Ge(111) to the experimental result, the tail of the calculated yield spectrum for both  $\text{He}^+$  and  $\text{Ne}^+$  shifts to lower energies, slightly below the tail of the experimental spectrum. For Si(111) the difference between the calculated

and experimental work function is smaller, leading to only a minor shift in the spectra. It should be noted that although the use of the experimental work function leads to an improvement of the calculated yield spectra for the results presented here, the experimental results for the work function can vary significantly, approximately with the same magnitude as the expected inaccuracy on *ab initio* calculated work functions [33]. Because the calculation of the SEE yield is sensitive to the vacuum level, the difficulty in accurately determining the work function adds another challenge to the calculation of the ion-induced emission coefficient  $\gamma$ .

In order to determine the contribution of the electron cascade process, Fig. 4 also shows the yield spectrum of the initial neutralization step, i.e., without adding any of the escaped electrons due to electron cascades. For all of the ion-surface combinations, the electron cascades increase the number of low energy electrons substantially. Hence, by considering electron cascades, we can obtain the missing low energy electrons in Hagstrum's original approach, without introducing a large anisotropy in the initial direction of the excited electrons. If we look at the fraction  $f_c$  of the contribution of the electron cascades to the final SEE

TABLE I. Calculated work functions  $\phi$ , compared with those calculated by De Waele *et al.* ( $\phi_{\text{ref}}$ ) [40] and experimental values ( $\phi_{\text{exp}}$ ).

Surface	$\phi$ (eV)	$\phi_{\text{ref}}$ (eV)	$\phi_{\text{exp}}$ (eV)
Ge(111)	4.548	4.569	5.00 <sup>a</sup>
Si(111)	4.902	4.889	4.79 <sup>b</sup>

<sup>a</sup>Polycrystalline sample from Michaelson [38].

<sup>b</sup>Averaged value from Kawano [39].

TABLE II. Calculated yield  $\gamma$ , compared with the experimental values of Hagstrum ( $\gamma_{\text{exp}}$ ) [6]. The fraction  $f_c$  of the contribution of the electron cascade process to the total yield, expressed as a percentage, as well as the calculated yield using the experimental work function  $\gamma_\phi$  are also tabulated.

Surface	Ion	$\gamma$	$f_c$ (%)	$\gamma_\phi$	$\gamma_{\text{exp}}$
Ge(111)	He <sup>+</sup>	0.205	41	0.156	0.196
	Ne <sup>+</sup>	0.125	28	0.102	0.138
Si(111)	He <sup>+</sup>	0.166	32	0.176	0.188
	Ne <sup>+</sup>	0.100	22	0.106	0.128

yield (Table II), we can see that on average approximately 31% of the total yield is a result of electron cascade process. Moreover, the contribution is higher for Ge than for Si, most likely due to the larger band gap of Si, which results in a larger minimum energy loss for the scattered electrons. The higher value of  $f_c$  for He<sup>+</sup> impact compared to Ne<sup>+</sup> is because the larger ionization energy of He<sup>+</sup> allows for more iterations in the electron cascade process.

However, when the high energy tail of the the yield spectrum is reproduced accurately, the model still underestimates the yield spectra. This can in part be explained by the anisotropy of the system caused by the incoming ion, which means that the distribution of the direction of the wave vectors  $P_\Omega(\varepsilon)$  is most likely not fully isotropic. This was Hagstrum's motivation for introducing the  $\alpha$  and  $\beta$  parameters, in order to skew the direction of the excited electrons towards the surface. Our results indicate that Hagstrum most likely overestimated the anisotropy when fitting these parameters, as he did not consider the contribution of the electron cascades to the yield spectrum. However, the fact that we adopt an isotropic distribution could explain the underestimation of the yield in the results. Second, considering the matrix elements to be constant means that we treat all electronic energy levels on an equal footing. It is possible that including the calculation of the matrix elements could result in an increased participation of high energy electrons in the Auger neutralization, producing excited electrons with higher average energies. This extra energy would be passed on in the cascade process and hence result in an increase of the overall yield. The fact that our results match fairly well with experiment, however, is an indication that this effect would likely be small and that

considering the matrix elements to be constant is a reasonable approximation for Ge and Si.

## V. CONCLUSIONS AND OUTLOOK

Starting from Hagstrum's model, we have presented a method for calculating the SEE yield of incoming ions on semiconductor surfaces and have applied it to incident He<sup>+</sup> and Ne<sup>+</sup> ions on the (111) surface of Ge and Si. By determining the required input using *ab initio* DFT calculations, as well as using a different expression for the escape function, we have eliminated the parameters Hagstrum used in his model. Furthermore, we have implemented the concept of electron cascades, obtaining the low energy electrons missing in our initial spectra. Using this approach, we have found spectra that match closely to experiment, both in shape as well as the total calculated yield.

Calculating accurate SEE yield coefficients from first principles is a challenging undertaking, both due to the complexity of the processes involved, as well as their sensitivity to the vacuum level. Although our model gives good results for Ge and Si, more experimental data on the ion-induced electron emission from semiconductors would provide a valuable opportunity to further validate our approach. In a next step, we can also extend the application of our model to metals, for which more experimental results are available. However, it is well known that plasmon excitations play an important role in the interaction of ions and metallic surfaces [19,41,42], so any attempt to calculate  $\gamma$  for metals would have to include a suitable implementation of collective excitations of the electrons in the surface. We aim to introduce such an extension of our model in a forthcoming paper.

## ACKNOWLEDGMENTS

We would like to thank Prof. D. Depla for the useful discussions on the secondary electron yield. Furthermore, we acknowledge financial support of FWO-Vlaanderen through project G.0216.14N. The computational resources and services used in this work were provided by the VSC (Flemish Supercomputer Center) and the HPC infrastructure of the University of Antwerp (CalcUA), both funded by the FWO-Vlaanderen and the Flemish Government-department EWI.

- 
- [1] D. Depla, G. Buyle, J. Haemers, and R. De Gryse, *Surf. Coat. Technol.* **200**, 4329 (2006).
  - [2] D. Depla, S. Mahieu, and R. De Gryse, *Thin Solid Films* **517**, 2825 (2009).
  - [3] Y. Motoyama and F. Sato, *IEEE Trans. Plasma Sci.* **34**, 336 (2006).
  - [4] Y. Cho, C. Kim, H.-S. Ahn, E. Cho, T.-E. Kim, and S. Han, *J. Appl. Phys.* **101**, 083710 (2007).
  - [5] H. D. Hagstrum, *Phys. Rev.* **89**, 244 (1953).
  - [6] H. D. Hagstrum, *Phys. Rev.* **119**, 940 (1960).
  - [7] P. S. Kothnur, X. Yuan, and L. L. Raja, *Appl. Phys. Lett.* **82**, 529 (2003).
  - [8] M. J. Kushner, *J. Phys. D: Appl. Phys.* **38**, 1633 (2005).
  - [9] H. D. Hagstrum, *Phys. Rev.* **96**, 336 (1954).
  - [10] H. D. Hagstrum, *Phys. Rev.* **122**, 83 (1961).
  - [11] F. M. Propst, *Phys. Rev.* **129**, 7 (1963).
  - [12] A. A. Almulhem and M. Girardeau, *Surf. Sci.* **210**, 138 (1989).
  - [13] N. Lorente, R. Monreal, and M. Alducin, *Phys. Rev. A* **49**, 4716 (1994).
  - [14] R. Monreal and N. Lorente, *Phys. Rev. B* **52**, 4760 (1995).
  - [15] R. C. Monreal, *Prog. Surf. Sci.* **89**, 80 (2014).
  - [16] J. Burgdörfer and C. Lemell, in *Slow Heavy-Particle Induced Electron Emission from Solid Surfaces* (Springer, Berlin, Heidelberg, 2007), pp. 1–38.
  - [17] F. Aumayr and H. Winter, in *Slow Heavy-Particle Induced Electron Emission from Solid Surfaces* (Springer, Berlin, Heidelberg, 2007), pp. 79–112.
  - [18] A. Cobas and W. E. Lamb, *Phys. Rev.* **65**, 327 (1944).

- [19] R. A. Baragiola and C. A. Dukes, *Phys. Rev. Lett.* **76**, 2547 (1996).
- [20] P. Riccardi, A. Sindona, P. Barone, A. Bonanno, A. Oliva, and R. Baragiola, *Nucl. Instrum. Methods Phys. Res., Sect. B* **212**, 339 (2003).
- [21] D. Goebel, D. Valdés, E. Abad, R. C. Monreal, D. Primetzhofer, and P. Bauer, *Phys. Rev. B* **84**, 165428 (2011).
- [22] D. Goebel, D. Roth, D. Primetzhofer, R. C. Monreal, E. Abad, A. Putz, and P. Bauer, *J. Phys. Condens. Matter* **25**, 485006 (2013).
- [23] D. Valdés, J. M. Blanco, V. A. Esaulov, and R. C. Monreal, *Phys. Rev. Lett.* **97**, 047601 (2006).
- [24] G. Kresse and J. Hafner, *Phys. Rev. B* **47**, 558 (1993).
- [25] G. Kresse and J. Hafner, *Phys. Rev. B* **49**, 14251 (1994).
- [26] G. Kresse and J. Furthmüller, *Comput. Mater. Sci.* **6**, 15 (1996).
- [27] G. Kresse and J. Furthmüller, *Phys. Rev. B* **54**, 11169 (1996).
- [28] P. E. Blöchl, *Phys. Rev. B* **50**, 17953 (1994).
- [29] G. Kresse and D. Joubert, *Phys. Rev. B* **59**, 1758 (1999).
- [30] J. P. Perdew, K. Burke, and M. Ernzerhof, *Phys. Rev. Lett.* **77**, 3865 (1996).
- [31] H. J. Monkhorst and J. D. Pack, *Phys. Rev. B* **13**, 5188 (1976).
- [32] See Supplemental Material at <http://link.aps.org/supplemental/10.1103/PhysRevB.99.085413> for more details on the first-principles calculations.
- [33] S. De Waele, K. Lejaeghere, M. Sluydts, and S. Cottenier, *Phys. Rev. B* **94**, 235418 (2016).
- [34] R. A. Baragiola, *Nucl. Instrum. Methods Phys. Res., Sect. B* **78**, 223 (1993).
- [35] M. O. Aboelfotoh and J. A. Lorenzen, *J. Appl. Phys.* **48**, 4754 (1977).
- [36] S. J. Yoon, I. Lee, J.-W. Lee, and B. Oh, *Jpn. J. Appl. Phys.* **40**, 809 (2001).
- [37] N. Lorente, R. Monreal, and M. Maravall, *Nucl. Instrum. Methods Phys. Res., Sect. B* **100**, 290 (1995).
- [38] H. B. Michaelson, *J. Appl. Phys.* **48**, 4729 (1977).
- [39] H. Kawano, *Prog. Surf. Sci.* **83**, 1 (2008).
- [40] S. De Waele (private communication).
- [41] R. A. Baragiola, C. A. Dukes, and P. Riccardi, *Nucl. Instrum. Methods Phys. Res., Sect. B* **182**, 73 (2001).
- [42] R. A. Baragiola and R. C. Monreal, in *Slow Heavy-Particle Induced Electron Emission from Solid Surfaces* (Springer, Berlin, Heidelberg, 2007), pp. 185–211.